Research Progress of Multi-aperture Laser Transceiving Control for Beam Combining Applications in IOE, CAS

Feng Li[1,2], Xinyang Li[1,2,*], Chao Geng[1,2], Guan Huang[1,2,3] and Yan Yang[1,2,3]

[1]Institute of Optics and Electronics, Chinese Academy of Sciences, Chengdu, Sichuan 610209, China
[2]Key Laboratory on Adaptive Optics, Chinese Academy of Sciences, Chengdu, Sichuan 610209, China
[3]University of Chinese Academy of Sciences, Beijing 100049, China

Keywords: Multi-aperture Laser Transceiving, Beam Combining, Adaptive Fiber Coupling.

Abstract: Nowadays, the development of fiber laser beam combining faces new challenges during propagating through the real long-range atmosphere. Aberrations in such transmission systems include turbulence-induced dynamic aberrations located at the path from the fiber laser array to the target, besides the inherent phase errors like phase noises and tip/tilt errors. Existing techniques, e.g., target-in-the-loop and delayed stochastic parallel gradient descent, are difficult to deal with the fast-changing turbulence-induced tip/tilt aberrations. But correcting these aberrations is critical for obtaining combined laser beams on the target with the best beam quality. In this paper, research progress of multi-aperture laser transceiving control for beam combining applications in IOE, CAS is presented. These novel techniques presented here provide efficient ways to achieve tip/tilt control for the beam coupling from space to fiber and the outgoing laser beams in the beam combining applications.

1 INTRODUCTION

Fiber laser techniques have been under intensive investigations for their excellent beam quality, high efficiency and flexible structure. While, single fiber laser beam with high power and good beam quality simultaneously is hard to achieve, owing to physical limits like nonlinear effect, thermally-induced modal instability, and thermal damage (Yu et al., 2011). Coherent beam combining (CBC) gives excellent solutions to these hard issues and shows great prospects in laser systems like directed energy, free space laser communications, and laser radar. Tiled beam array and filled-aperture are the two main architectures of fiber laser CBC. Compared with the later one, tiled beam array method not merely provides a flexible method producing high power output with excellent beam quality, but also could act as a scalable fiber laser transceiver. Recently developed coherent tiled fiber laser arrays composed of numerous fiber collimators have aroused a significant interest (Weyrauch et al., 2011). In such systems, traditional and monolithic large-aperture transmitters are replaced by smaller sub-aperture array for improved adaptive optics (AO) performance. The phase distortions in these systems

are divided into piston and/or tip/tilt errors within the sub-apertures (Filimonov et al., 2014). Benefited from the mature fiber-integrated phase devices, issues about piston errors have been widely researched and well solved. Meanwhile, novel device named adaptive fiber-optics collimator (AFOC) has been invented to manipulate the tip/tilt phases in fiber laser CBC systems (Liu et al., 2007 and Geng et al., 2013). Compared to conventional tip/tilt devices like FSM, the AFOC drives fiber tip directly to execute tip/tilt. Such devices are with advantages of precise control, small inertia, high resonance frequency and convenience for assembling and integration (Lachinova et al., 2008).

Further development of the tiled beam array (or fiber laser array) aims at highly efficient propagation through the atmosphere, not merely realization of CBC indoor. Thus, correcting aberrations, especially the turbulence-induced aberrations located at the transmission path, is critical for obtaining the best beam quality and the highest power intensity on the target. Alleviating the sub-aperture averaged piston-type aberrations of the laser source and turbulence, which is named as phase locking, is the basic item for CBC under atmosphere. Beyond the piston-type aberrations, compensation of the higher order

43

aberrations within the sub-apertures is needed if we want to further improve the performance of CBC under the atmosphere. In fact, tip/tilt-type errors take up the most part (almost 87%) of the aberrations for Kolmogorov turbulence in each sub-aperture. Without the tip/tilt-type errors, CBC under atmosphere would be more efficient where higher target hit-spot brightness could be obtained with even less transmitted power (Vorontsov et al., 2016). But such goal is blocked by the available bandwidth of the tip/tilt devices and the performance of existing control algorithm. The appearance of AFOC has solved the bandwidth issues to a certain extent. In this case, the performance of the control algorithm becomes particularly important.

Different from the traditional AO control, where extra wavefront sensors (like Hartmann-Shack sensor) are needed to measure the monolithic wavefront actively, fiber laser arrays mostly depend on optimization algorithm for CBC owing to their discrete architecture. Phasing through target-in-the-loop (TIL) with hill-climbing type techniques (like stochastic parallel gradient descent, SPGD) is the main existing approach for current CBC under turbulence (Weyrauch et al., 2016). In these schemes, the power-in-the-bucket (*PIB*) metric, which represents the laser power backscattered by the size-limited target point and collected by a local telescope, is utilized for power-maximization. The tip/tilt control and the phase locking control are mixed together in such single metric optimization techniques. The hardest problem is that the available bandwidth of AFOC (no more than 5 kHz) is much less than that of the fiber-integrated phasing devices (up to GHz), while the channel number of the former is double of the latter one (Geng et al., 2011). Obviously, existing methods are not fit for fiber laser array CBC systems with fast-changing tip/tilt errors.

New techniques making the best use of the limited AFOC bandwidth are in urgent need. Recent progress on techniques of adaptive fiber coupling reported by IOE, CAS gives out new ideas on such issues (Luo et al., 2014). In these methods, the fiber coupling efficiency of the modified AFOC could be improved with active tip/tilt-type phase errors control. Tip/tilt control for both the coupling from space to fiber and the outgoing laser beam is obtained. Such techniques achieve parallel tip/tilt control for each sub-aperture of the array, which is independent from the phase control in the CBC systems. In this paper, the research progress of multi-aperture laser transceiving control for beam combining applications in IOE, CAS is presented.

2 ADAPTIVE FIBER COUPLING

Here, we present the recent work of extending the control bandwidth of the AFOC for adaptive fiber coupling. An improved SPGD algorithm named precise-delayed SPGD (PD-SPGD) is proposed for the AFOC-based adaptive coupling system.

Figure 1 shows the structural scheme of the AFOC coupling system. A uniform plane wave laser beam is focused and coupled into the single-mode-fiber (SMF) tip in the AFOC, part of the coupled optical energy is sent to a terminal receiver and the other part is detected by a photodetector (PD). The PD voltage is utilized as the performance metric of the control algorithm. Two-channel control signals from the controller are amplified by high-voltage amplifiers (HVAs) and then drive the AFOC for closed loop control.
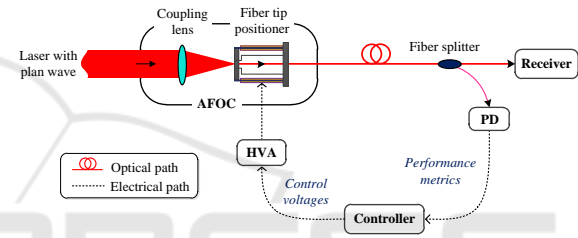

Figure 1: Structural scheme of adaptive coupling system based on AFOC.

Response delay between the input and the output is one of the key issues in almost all practical control systems. Parameter τ_{resp} is defined here as the delay between the change of the control voltage and the response of the metric and τ_{SPGD} as the period of a SPGD iterative cycle. Through massive experiments, we find that τ_{resp} keeps constant when the frequency is below 10 kHz. The average value is about 0.1 ms for both the X-direction and Y-direction of the AFOCs. Such inherent response delay will lead to inaccurate gradient estimation through the fast iterative process of SPGD algorithm where τ_{SPGD} becomes less than τ_{resp}. For example, when τ_{SPGD} is less than 0.2 ms, metric $J_-^{(n)}$ and $J_+^{(n)}$ of the SPGD algorithm is almost totally determined by the drive voltages of $U^{(n)}+\Delta U^{(n)}$ and $U^{(n-1)}-\Delta U^{(n-1)}$ respectively (n represents the time point). This will lead to opposite gradient estimation results if traditional SPGD algorithm is utilized as:

$$U^{(n+1)} = U^{(n)} + \gamma \Delta U^{(n)} \left(J_+^{(n)} - J_-^{(n)} \right) \qquad (1)$$

where γ is the gain coefficient.

So, readjustment of the correspondence between the metric and the disturbed voltage is needed, and

one way that might work is to set a controllable time delay. This idea originates from the delayed-SPGD (D-SPGD) algorithm, which has been successfully used to compensate the time delay caused by the optical wave propagation in CBC experiments (Weyrauch et al., 2016). Such improved algorithm is named as Precise-Delayed SPGD algorithm (PD-SPGD) here. The iterative procedure of the control voltage during each iteration cycle (n) can be described by the following rule:

$$U^{(n+1)} = U^{(n)} + \gamma \Delta U^{(n-\Delta n)} \left(J_i^{(n-\Delta n)} - J_{i+N/2}^{(n-\Delta n)} \right) \qquad (2)$$

where $i = 0, 1, ..., MN$. Here, the integer number $\Delta n = M$-1 is the integral-delay parameter and $i \geq 0$ is the precise-delay parameter that accounts for the response delay τ_{resp}. N is the number of sampling points of metrics within one time of iteration, which determines the accuracy of the compensation that can be achieved.
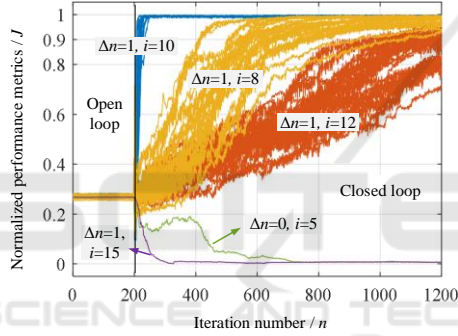

Figure 2: Iteration curve of different delay parameter settings in the experiment of static angular error correction.

Figure 2 shows the experimental results of fiber coupling with 367 μrad static angular error (almost misalignment of 5.5 μm at the fiber end). The iteration rate of the PD-SPGD algorithm is 8 kHz and the sampling rate is 80 kHz, thus τ_{SPGD}=0.125 ms, N=10. To compensate the response delay (96 μs), τ_{comp} is set to 0.127 ms, the integral delay parameter Δn=1 and the precise delay parameter i=10 (the closest integer number to 0.127/0.125 and 10×0.127/0.125 correspondingly). As shown in Figure 2, the iteration curve diverges when Δn=0 and i=5. When parameters Δn=1 and i=8, 10, 12 (the corresponding actual compensation time is 0.1 ms, 0.125 ms and 0.15 ms), the algorithm starts to converge and corresponding convergence time t_c (equal to the time needed for the normalized metric rise to 90%) is 55 ms, 2.5 ms and 137.5 ms through statistics of 20 sets of data. Finally, when Δn=1 and

i=15 (equivalent to using the D-SPGD algorithm), the iteration cure diverges again.

Sine angular jitter with frequency of 100 Hz and amplitude of 166 μrad is loaded on the plane wave and corresponding experimental results of SMF adaptive coupling using SPGD and PD-SPGD are shown in Figure 3. Iterative rates of these two algorithms are 3 kHz and 8 kHz respectively. Control parameters of both algorithms are carefully tested and optimized. The metric is with an average value of 0.81 and mean square error (MSE) of 0.13 under open loop. The average metric decreases to 0.79 and the MSE increases to 0.14 when SPGD algorithm is utilized. The average metric increases to 0.97 and the MSE decreases to 0.019 when SPGD algorithm executes. SPGD becomes invalid under such circumstances, while PD-SPGD still works fine.

Above results reveal that the PD-SPGD algorithm proposed here has less convergence time and could get better performance than conventional SPGD algorithm. Meanwhile, this improved algorithm competently deals with dynamic tip/tilt errors with frequency approximating one hundred Hz, which shows potential abilities when facing turbulence-induced dynamic aberrations.
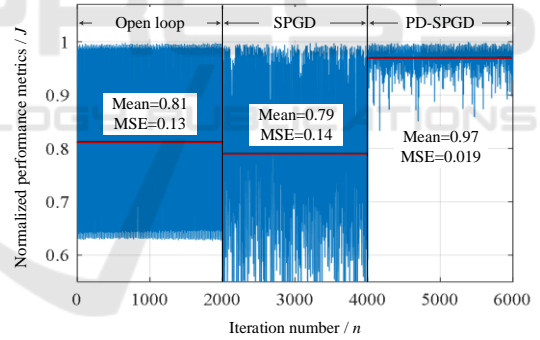

Figure 3: Comparison between the SPGD and PD-SPGD algorithm when the frequency of sine angular jitter is 100 Hz.

3 CO-APERTURE TRANSCEIVING OF TWO COMBINED BEAMS

The amount of the coupled power that enters to the SMF in the AFOC is inversely proportional to the displacement of the fiber-tip center in respect to the focal-spot centroid position of the incident beam. The pitch between the delivery fiber tip and the focal spot center is caused by the wavefront tip/tilt

aberrations. According to the principle of optical reciprocity, when the received optical wave power is maximized through the AFOC control, the tip/tilt errors are equivalently corrected for the counter-propagating outgoing and received laser beams in the delivery fiber. These two laser beams could share the same optical fiber path with help of directional fiber circulators or free-space fiber isolators. Meanwhile, for CBC with multi-AFOCs, such tip/tilts control could work in parallel for each single aperture. That means the tip/tilts control keeps two dimensional regardless of the scale of the CBC array.

Here, the current work about the co-aperture fiber laser transceiving propagation using AFOCs for both coupling and collimating in IOE, CAS are presented (Li et al., 2015). Fiber laser array composed of two-element AFOCs is built up and indoor simulated turbulence is set to introduce aberrations. SPGD algorithm is employed here to promote the fiber coupling efficiency and the combining efficiency of the fiber-array outgoing beams.
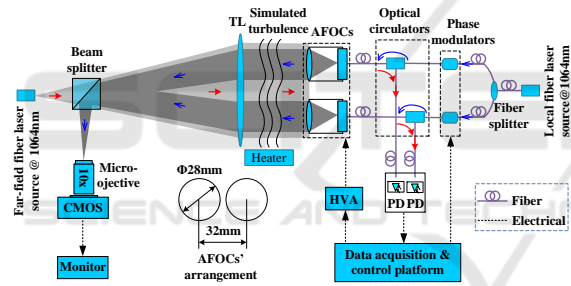

Figure 4: Experimental setup. PD: photo-detector. HVA: high voltage amplifier. TL: transform lens.

Experimental setup of the co-aperture laser beam transceiving propagation is illustrated in Figure 4. A transform lens (TL) is employed to simulate the optical far-field. A fiber laser with the fiber tip located at the far-field is set to be as the unresolved target and the target source. The target outgoing beam is collimated by the TL, and heated to generate the atmospheric turbulence aberrations. Then, the phase-distorted collimating beam is focused and coupled into the internal polarization-maintaining fibers (PMFs) of the AFOC array separately. The coupled beams are detected by PDs. At the same time, the local collimated fiber laser beams from the two AFOCs are also heated to generate conjugated aberrations. The two phase-distorted sub-beams are focused by the TL, and then detected by a high speed CMOS camera for observation.

The iteration rate of the SPGD algorithm is about 1.15 kHz. Figure 5 (a) and Figure 5 (b) show the evolution curves of coupling power of the AFOCs, denoted as P_1 and P_2, when tip/tilt control is off and on under the influences of simulated turbulence. Here, P_1 and P_2 are normalized by the maximum value in respective closed loop. Duration of both the open and closed states is all about 12-second. The average value of P_1 for one AFOC increases from 0.61 in open loop to 0.85 in closed loop, and the *MSE* drops from 0.16 to 0.048. For P_2, the average value increases from 0.57 to 0.85 and the *MSE* drops from 0.14 to 0.04 correspondingly. The results indicate that the efficiency of coupling laser beam with distorted wave-front from space into PMF can be effectively promoted through tip/tilt error control with AFOCs.
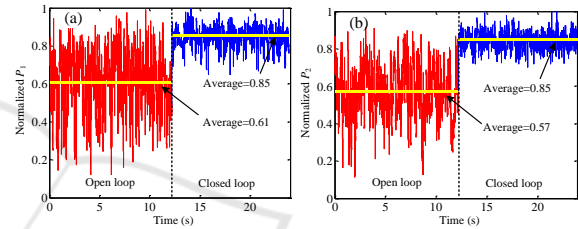

Figure 5: Evolution curves of the coupled laser power normalized by the maximum value in separately closed loop. (a) Received by AFOC-1. (b) Received by AFOC-2.
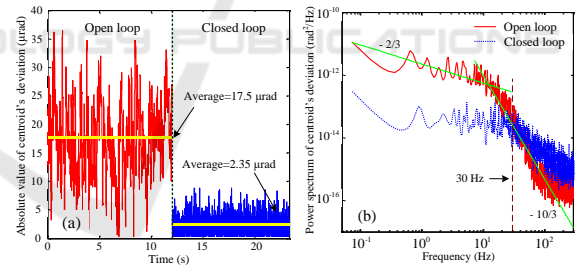

Figure 6: Combination of the two AFOC-collimating beams in the far-field. (a) The absolute-value evolution curve of the diffraction pattern centroid's deviations. (b) Frequency spectrum-density distribution of the curve in (a).

Figure 6 (a) depicts the absolute-value evolution curve of the diffraction pattern centroid's deviations of the two AFOC-collimating beams in the far-field. The average absolute-value of the centroid's deviation drops from 17.5 µrad in open loop to 2.35 µrad in closed loop, the *MSE* value drops from 6.59 µrad to 1.35 µrad, and the peak-valley value drops from 36.8 µrad to 8.54 µrad (the diffraction-limited angle of a single AFOC aperture is about 92 µrad). Figure 6 (b) describes the frequency spectrum-

density distributions of the open and closed loop curves in Figure 6 (a), respectively. Deviations of less than 30 Hz have been well corrected. The results show that the tip/tilt errors of the outgoing laser beams are equivalently corrected when the received optical wave power is maximized.

4 CBC BASED ON 7-APERTURE LASER TRANSCEIVING

Experiment in part 3 is focused on the tip/tilt aberrations correction and the piston aberrations are not considered in. However, phase-locking is the basic condition for CBC. To obtain CBC of the AFOC array, tip/tilt control with adaptive fiber coupling is cooperated with the TIL-based phasing techniques. Here we present the researches about CBC based on multi-aperture laser transceiving in IOE, CAS (Li et al., 2017).
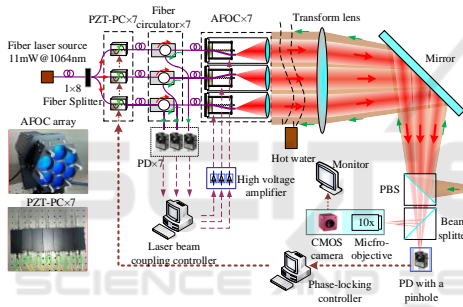

Figure 7: Experimental setup of CBC based on 7-aperture laser transceiving. PZT-PC: piezoelectric-ceramic-ring fiber-optic phase compensator. AFOC: adaptive fiber-optics collimator. PD: photo detector. PBS: polarized beam splitter.

Fiber laser CBC experiment setup with AFOC array of seven sub-apertures is illustrated in Figure 7. Polarized and single-frequency fiber laser beams from the 7-subaperture AFOC array are heated by hot water to bring in simulated dynamic turbulence aberrations and focused by a transform lens. Then the focused beamlets are detected by a PD with a pinhole for phase-locking control (PL) and a high-speed CMOS camera for observation simultaneously. Piezoelectric-ceramic-ring fiber-optic phase compensators (PZT PC) are utilized here to correct the piston-type errors of the array. A pigtail fiber with its end located in the focal spot of the transform lens is used as a simulated objective in the far-filed. The monolithic-beam from the fiber tip is collimated by the transform lens and cut off by the array, and then focused and coupled into the PMFs of each

AFOC respectively. Metrics detected by each PD are utilized for tip/tilt control (TT) for each AFOC in parallel.
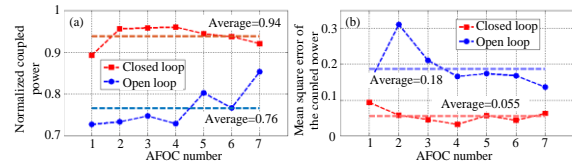

Figure 8: Average (a) and mean square error (b) of the normalized coupled power for each AFOC when TT control is in open loop and closed loop.

The average normalized coupled power for all the seven AFOCs is about 0.76 without TT control and then increases to 0.94 when TT control is brought in as shown in Figure 8 (a). The average *MSE* of the coupled power for all the seven AFOCs is about 0.18 in open loop and then turns to 0.055 in closed loop as illustrated in Figure 8 (b).
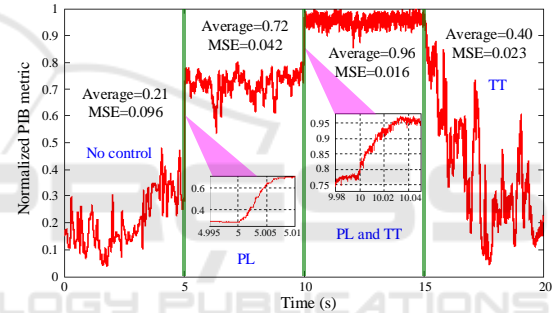

Figure 9: The normalized PIB metrics acquired by PD as the function of time.

Figure 9 shows the normalized *PIB* metric acquired from the PD as the function of time during four stages, which are no control stage, PL stage, PL and TT stage, and single TT stage. The *PIB* metric is normalized via being divided by the maximum PIB during each stage. Without any control, the mean *PIB* metric is just 0.21 and the corresponding *MSE* is 0.096 due to the simulated turbulence and the phase noise of the transmission fibers. When only PL control turns on, the *PIB* metric is locked at a higher value with an average of 0.72, which is 3.4 times of that for no control stage. Meanwhile, the *MSE* decreases to 0.042. Then the TT control is brought in and the *PIB* metric is further optimized. The metric is with an average of 0.96 and *MSE* of 0.016, which is only 1/6 of that in the no control stage. The convergence of the adaption process after the TT control is switched on takes time about 30 ms, which equals to the time that each AFOC needs to maximize the coupled power. Such results indicate

that we realizes the parallel tip/tilt control for each AFOC and such control is independent from the phase locking, which is quite different from the existing techniques.
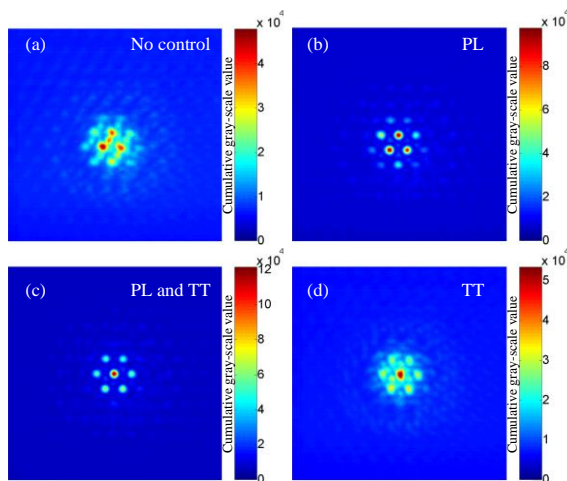

Figure 10: The long-exposure far-field intensity distributions. (a) No control. (b) PL control. (c) PL and TT control. (d) TT control.

The long-exposure far-field intensity distributions during the four control stages are shown in Figures 10(a-d), respectively. The long-exposure pattern is diffused by the simulated turbulence and the fringe visibility is very weak when no control is implemented. Fringe contrast increases when PL works. Due to the simulated turbulence and the initial static pointing errors of the AFOCs during assembling, intensity of the side lobes located bellow the main lobe approximates that of the main lobe when only PL control works. Further pre-compensation of the tip/tilt-type errors through the TT control could resolve such issues and results in pattern (Figure 10 (c)) comparable with the ideal pattern. Sole TT control just benefits the intensity of the central point, but not the fringe contrast (Figure 10 (d)). All the results above indicate that excellent fiber laser array CBC under simulated turbulence has been achieved through the cooperation of the tip/tilts correction based on multi-aperture laser transceiving control and the active phase locking control.

5 CONCLUSIONS

Future CBC of the tiled fiber laser array aims at efficient transmission under atmosphere, which will inevitably face challenges of alleviating the turbulence-induced dynamic aberrations distributed in the whole array aperture. Existing research results mainly based on TIL and optimization algorithms suffer from the defects of poor bandwidth utilization efficiency, especially for the bandwidth-limited tip/tilt devices represented by AFOCs. To solve these issues, techniques of multi-aperture laser transceiving control have been developed by IOE, CAS. Such methods give abilities of efficient and parallel adaptive correction to the tiled fiber laser array. Research progresses on improved SPGD algorithm of fiber coupling, co-aperture transceiving of fiber laser array with adaptive tip/tilts corrections, and CBC of tiled fiber laser array are presented. Excellent results indicate the potential applications of such techniques in fiber coupling, laser communication and beam projection applications.

REFERENCES

Yu, C. X., Augst, S. J., Redmond, S. M., 2011. Coherent combining of a 4kW, eight-element fiber amplifier array. *Opt. Lett. 36/14*, 2686-2688.

Weyrauch, T., Vorontsov, M. A., Carhart, G. W., Beresnev, L. A., Rostov, A. P., Polnau, E. E., Liu, J. J., 2011. Experimental demonstration of coherent beam combining over a 7 km propagation path. *Opt. Lett. 36/22*, 4455-4457.

Filimonov, G. A., Vorontsov, M. A., Lachinova, S. L., 2014. Performance analysis of a coherent tiled fiber-array beam director with near-field phase locking and programmable control of tip/tilt and piston phases. *Proc. SPIE 8971/9*, 1-6.

Liu, L., Vorontsov, M. A., Polnau, E., Weyrauch, T., Beresnev, L. A., 2007. Adaptive phase-locked fiber array with wavefront phase tip-tilt compensation using piezoelectric fiber positioners. *Proc. SPIE 6708/0K*, 1-12.

Geng, C., Luo, W., Tan, Y., Liu, H., Mu, J., Li, X., 2013. Experimental demonstration of using divergence cost-function in SPGD algorithm for coherent beam combining with tip-tilt control. *Opt. Express 21/21*, 25045–25055.

Geng, C., Zhao, B., Zhang, E., Luo, W., Tan, Y., Zhu, Y., Yang, H., Mu, J., Li, X., Duan, K., Zhao, W., 2013. 1.5 kW Incoherent beam combining of four fiber lasers using adaptive fiber-Optics collimators. *IEEE Photon. Technol. Lett. 25/13*, 1286-1289.

Lachinova, S. L., Vorontsov, M. A., 2008. Laser beam projection with adaptive array of fiber collimators. II. Analysis of atmospheric compensation efficiency. *J. Opt. Soc. Amer. A 25/8*, 1960–1973.

Vorontsov, M. A., Filimonov, G., Ovchinnikov, V., Polnau, E., Lachinova, S. L., Weyrauch, T., Mangano, J., 2016. Comparative efficiency analysis of fiber-array and conventional beam director systems in volume turbulence. *Appl. Opt. 55/15*, 4170–4185.

Weyrauch, T., Vorontsov, M. A., Mangano, J., Ovchinnikov, V., Bricker, D., Polnau, E. E., Rostov, A. P., 2016. Deep turbulence effects mitigation with coherent combining of 21 laser beams over 7 km. *Opt. Lett. 41/4*, 840-843.

Geng, C., Li, X., Zhang, X., Rao, C., 2011. Coherent beam combination of an optical array using adaptive fiber optics collimators. *Opt. Commun. 284/24*, 5531–5536.

Luo, W., Geng, C., Wu, Y., Tan, Y., Luo, Q., Liu, H., Li, X., 2014. Experimental demonstration of single-mode fiber coupling using adaptive fiber coupler. *Chin. Phys. B 23/1*, 014207.

Li, F., Geng, C., Li, X., Qui, Q., 2015. Co-aperture transceiving of two combined beams based on adaptive fiber coupling control. *IEEE Photon. Technol. Lett. 27/17*, 1787–1790.

Li, F., Geng, C., Huang, G., Yang, Y., Li, X., Qui, Q., 2017. Experimental demonstration of coherent combining with tip/tilt control based on adaptive space-to-fiber laser beam coupling. *IEEE Photon. J. 9/2*, 7102812.